Origin of Insulating Ferromagnetism in Iron Oxychalcogenide $Ce_2O_2FeSe_2$

Ling-Fang Lin,[1] Yang Zhang,[1] Gonzalo Alvarez,[2] Adriana Moreo,[1,3] and Elbio Dagotto[1,3]
[1]*Department of Physics and Astronomy, University of Tennessee, Knoxville, Tennessee 37996, USA*
[2]*Computational Sciences and Engineering Division and Center for Nanophase Materials Sciences, Oak Ridge National Laboratory, Oak Ridge, Tennessee 37831, USA*
[3]*Materials Science and Technology Division, Oak Ridge National Laboratory, Oak Ridge, Tennessee 37831, USA*

(Received 17 May 2021; revised 16 July 2021; accepted 19 July 2021; published 13 August 2021)

An insulating ferromagnetic (FM) phase exists in the quasi-one-dimensional iron oxychalcogenide $Ce_2O_2FeSe_2$, but its origin is unknown. To understand the FM mechanism, here a systematic investigation of this material is provided, analyzing the competition between ferromagnetic and antiferromagnetic tendencies and the interplay of hoppings, Coulomb interactions, Hund's coupling, and crystal-field splittings. Our intuitive analysis based on second-order perturbation theory shows that large entanglements between doubly occupied and half filled orbitals play a key role in stabilizing the FM order in $Ce_2O_2FeSe_2$. In addition, via many-body computational techniques applied to a multiorbital Hubbard model, the phase diagram confirms the proposed FM mechanism.

DOI: 10.1103/PhysRevLett.127.077204

Introduction.—The understanding of the superexchange phenomenon in transition metal compounds continues attracting the attention of the condensed matter community [1–4]. Superexchange theory based on atomic-limit second-order perturbation theory in the hopping amplitudes dominates for many insulators [1–3]: as illustrated in Fig. 1(a), the Heisenberg coupling between two half filled orbitals is antiferromagnetic (AFM). However, via third-order perturbation theory, the case involving half filled and empty orbitals, coupled with partially filled orbitals via Hund's coupling J_H, Fig. 1(b), leads to ferromagnetic (FM) order instead. Being third order, the FM coupling magnitude is smaller than the AFM superexchange. Also at third order, the case involving fully filled and half filled orbitals, also coupled with partially filled orbitals via J_H, Fig. 1(c), should also be FM [2,5].

Generally, magnetic insulators exhibit multiple types of active interactions, including the kinetic exchange, normally AFM and dominant, and the direct exchange, normally FM and weak [1]. For stronger FM order, mechanisms such as double exchange are invoked, but the induced state is metallic [7,8]. Thus, the canonical stereotype is that magnetic insulators are primarily antiferromagnets and magnetic metals are primarily ferromagnets.

However, robust FM insulators are known experimentally, such as $BiMnO_3$ with orbital order [9], double perovskite Sr_3OsO_6 [10], 90° bond $CrSiTe_3$ [11], and others [12–21]. Materials with 180° and 90° bond cases can be qualitatively understood by the semiempirical Goodenough-Kanamori-Anderson (GKA) rules [1–3, 22–25]. But other cases are more challenging if the cation-anion-cation bond angle deviates substantially from 180° or 90°, or if the crystal-field symmetry of the magnetic ion is more complicated than in the octahedral coordination. The many FM insulators found experimentally suggest the GKA rules are probably incomplete.

In this Letter, we explain the FM insulating state in the quasi-one-dimensional (Q1D) $Ce_2O_2FeSe_2$ (COFS) material. The new concept we introduce is that, due to geometrical reasons, some of the *interorbital* electronic hopping amplitudes can become comparable, or even larger, than the intraorbital hoppings, allowing for FM order to dominate over AFM order. We show explicitly that for COFS, at robust J_H, remarkably FM order defeats AFM order, unveiling a noncanonical mechanism to generate a FM insulator. Our study only requires second-order perturbation theory and thus is directly comparable in magnitude to Anderson's superexchange.

Model system.—Low-dimensional materials and models attract considerable attention [26–37]. Experiments showed that Q1D COFS, structurally related to the *Ln*FeAsO family, has a large magnetic moment ~3.14–3.33 μ_B on

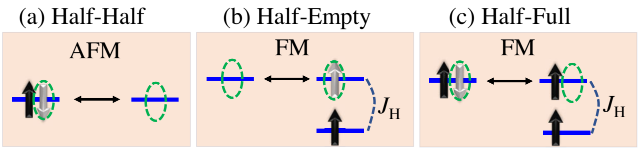

FIG. 1. Sketch of the basic superexchange cases known (a)–(c). Blue lines and black arrows represent the orbitals and electrons with spin up or down, respectively. The two-way thin arrows indicate the overlap between intersite orbitals. Gray thick arrows in the green dashed circles indicate virtual hopping processes. Real materials might host more than one exchange, introducing competition between them [6].

Fe^{2+} ($3d$ $n = 6$ electrons) and is ferromagnetically coupled along the dominant chain direction [38,39]. Each chain is made of distorted edge-sharing FeSe_4 tetrahedra and the Fe—Se—Fe bond is 71°, highly deviating from 90°. Experiments showed that the Fe—Se—Ce interactions are much weaker than the Fe-Se-Fe nearest-neighbor (NN) interactions. Thus, COFS is essentially a 1D chain system [39], with weak coupling between chains. The experimental gap ~0.64 eV shows this material is insulating [38]. Thus, COFS with robust magnetic order at 176 K is an excellent candidate to study deviations of the GKA rules to explain FM insulators.

Density functional theory (DFT) results.—From DFT [40–42], the band structure of the noninteracting nonmagnetic phase of COFS is more dispersive along the chain direction (Γ-X/S-Y path) than other directions, indicating dominant one-dimensional behavior along the k_x axis [Figs. 2(a)–2(c)]. Hopping amplitudes and crystal-field splitting energies for the five $3d$ iron orbitals were extracted using the maximally localized Wannier functions [43,44] and they are in Fig. 2(d). Including the Hubbard U and magnetism, experiments suggest that COFS should be a Mott insulator with no bands crossing the Fermi level.

As shown in Fig. 2(d), the orbital $d_{x^2-y^2}$ has the largest NN intraorbital hopping and the lowest on site crystal-field energy level. Besides the intraorbital hoppings, our results indicate that the interorbital hoppings—i.e., nonzero off-diagonal matrix elements—are also robust. These important interorbital hoppings lead to orbital entanglement. The five orbitals can be naturally divided into three sectors: sector 1 $\{d_{z^2}\}$ (primarily isolated), 2 $\{d_{x^2-y^2}, d_{yz}\}$, and 3 $\{d_{xz}, d_{xy}\}$. From the DFT hopping amplitudes and crystal fields, the total bandwidth for each sector is, roughly, ~1, 2.3, and 1 eV, respectively, with sector 2 having the largest bandwidth [45]. Note that Fig. 2(d) is only a sketch and should not be confused with the bands of Fig. 2(a).

If only the kinetic term and crystal-field splitting were included, i.e., at $U = 0$ and $J_H = 0$, sectors 2 and 3 will form entangled bonding and antibonding states with band gaps between them [Fig. 2(b)]. The six electrons would fill energy levels with three spins up and three spins down forming a nonmagnetic state, with electrons distributed in each sector as $\{2, 2, 2\}$, respectively. However, at large U and J_H [Fig. 2(e)] orbitals are decoupled and localized forming a Mott phase, and the six electrons fill energy levels with five spins up and one spin down, leading to a high-spin state. Electrons are distributed in each sector as $\{1, 3, 2\}$, respectively. The extra electron (pointing down) will be in orbital $d_{x^2-y^2}$, due to its lowest crystal-field energy. Because COFS is an insulator with Fe^{2+} in a high-spin state [38,39], from this analysis, the most relevant three orbitals are $\{d_{z^2}, d_{yz}, d_{x^2-y^2}\}$ from sectors 1 and 2 and are, thus, the basis in our Hamiltonian analysis below. Orbitals $\{d_{z^2}, d_{yz}, d_{x^2-y^2}\}$ are labeled $\{\gamma_0, \gamma_1, \gamma_2\}$ for simplicity.

Figures 2(f) and 2(g) provide an intuitive perspective of the effective orbitals and the overlaps between orbital γ_1 for Fe1 and γ_2 for Fe2. These effective orbitals are a combination of the Fe d and the Se p orbitals. The dominant overlaps are mainly contributed by the Se p orbitals; i.e., Se as the Fe—Fe bridge is crucial in the hybridization. A direct overlap between d orbitals is also observed, due to the short distance (~2.84 Å) between NN irons. The entanglements between orbitals, compatible with the large hopping t_{12}, plays a key role in COFS, as discussed below.

Hubbard model.—To understand the magnetism of COFS, a three-orbital Hubbard model for the Fe chain was constructed [46], including tight-binding kinetic energy and on site Coulomb interaction energy terms $H = H_k + H_{\mathrm{int}}$. The kinetic portion is

$$H_k = \sum_{i\sigma\gamma\gamma'} t_{\gamma\gamma'}(c^{\dagger}_{i\sigma\gamma} c_{i+1\sigma\gamma'} + \mathrm{H.c.}) + \sum_{i\sigma\gamma} \Delta_{\gamma} n_{i\sigma\gamma}, \qquad (1)$$

where the first term represents the electron hopping from orbital γ at site i to orbital γ' at the NN site $i + 1$. For simplicity, only the most important NN hopping amplitudes (eV units) are included [48],

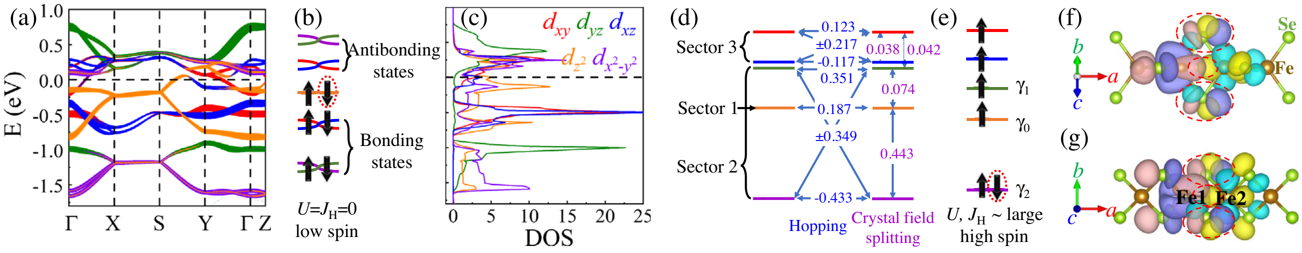

FIG. 2. (a) DFT iron $3d$ orbital-resolved band structure. (b) Sketches of bonding and antibonding states at small U and J_H and their close relation with the band structure in (a). The total population of electrons considered is six electrons to fill the energy levels (thick arrows). (c) DOS, from DFT calculations, for the nonmagnetic phase. (d) Crude sketches of the crystal-field splitting and dominant NN hopping parameters for the five orbitals. (e) Orbitals and their population at large U and J_H. The spin down marked with a dashed oval plays a key role in the FM mechanism described in this Letter. (f),(g) Effective Wannier functions (WFs) of orbital γ_1 for Fe1 (in pink and purple) and γ_2 for Fe2 (in blue and yellow). The robust overlap between these two WFs, related to the amplitude of hoppings t_{12}, are indicated by the dashed red ovals.

$$t_{\gamma\gamma'} = \begin{bmatrix} 0.187 & -0.054 & 0.020 \\ 0.054 & 0.351 & -0.349 \\ 0.020 & 0.349 & -0.433 \end{bmatrix}. \tag{2}$$

Δ_γ is the crystal-field splitting of orbital γ; i.e., $\Delta_0 = -0.277$, $\Delta_1 = -0.203$, and $\Delta_2 = -0.720$ eV, respectively. The total kinetic energy bandwidth W is 2.085 eV.

The model's electronic interaction—intraorbital Hubbard repulsion, interorbital repulsion at different orbitals, Hund's coupling, and pair hopping terms—is

$$H_{\mathrm{int}} = U\sum_{i\gamma} n_{i\uparrow\gamma}n_{i\downarrow\gamma} + \left(U' - \frac{J_H}{2}\right)\sum_{\substack{i \\ \gamma<\gamma'}} n_{i\gamma}n_{i\gamma'} - 2J_H\sum_{\substack{i \\ \gamma<\gamma'}} \mathbf{S}_{i,\gamma}\cdot\mathbf{S}_{i,\gamma'} + J_H\sum_{\substack{i \\ \gamma<\gamma'}} (P^{\dagger}_{i\gamma}P_{i\gamma'} + \mathrm{H.c.}), \tag{3}$$

where $U' = U - 2J_H$ is used and $P_{i\gamma} = c_{i\downarrow\gamma}c_{i\uparrow\gamma}$.

Second-order perturbation theory.—Consider the limit where the hoppings $t_{\gamma\gamma'} \ll U$, J_H are the perturbation. A sketch is in Fig. 3, considering two sites and three orbitals with population $\{1, 1, 2\}$ and focusing on the U, U', J_H, and Δ_γ terms (the pair hopping is widely considered to play a secondary role in calculations of this kind). For nondegenerate states, second-order perturbation theory to the ground state (state 1) always lowers the energy by

$$\Delta E_1 = -\sum_{m\neq 1}\frac{|\langle\psi^0_m|H'|\psi^0_1\rangle|^2}{E^0_m - E^0_1}. \tag{4}$$

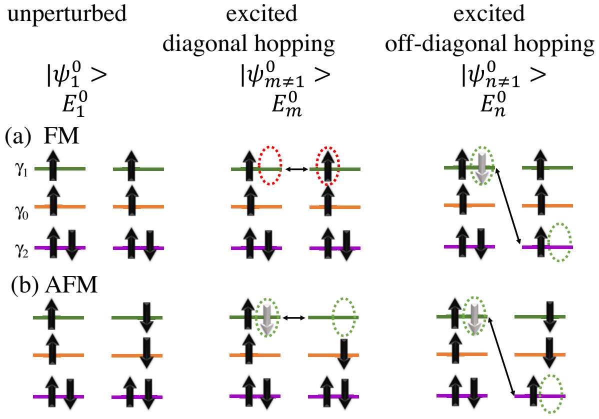

FIG. 3. Sketches of unperturbed and excited states for diagonal and off-diagonal hoppings. Both (a) FM and (b) AFM cases are considered. For the FM case, the diagonal hopping is forbidden (red ovals) due to the Pauli exclusion principle.

For both the FM and AFM unperturbed states, the ground state atomic energy is

$$E^0_1 = 2U + 10U' - 6J_H + 2\Delta_0 + 2\Delta_1 + 4\Delta_2. \tag{5}$$

(a) For the FM case, the intraorbital hopping is forbidden due to the Pauli principle. As for the excited state induced by the off-diagonal hopping, the energy is

$$E^0_{\mathrm{exc}} = 2U + 11U' - 7J_H + 2\Delta_0 + 3\Delta_1 + 3\Delta_2. \tag{6}$$

By using this second-order perturbation theory, the DFT-deduced hoppings and crystal fields, and the widely employed ratio $J_H/U = 1/4$ for iron superconductors, the total energy gain of the FM configuration due to t_{12} is

$$\Delta E_{\mathrm{FM}} = \frac{|\langle\psi^0_{\mathrm{exc}}|H'|\psi^0_1\rangle|^2}{E^0_1 - E^0_{\mathrm{exc}}} = -\frac{|t_{12}|^2}{U - 3J_H + \Delta_1 - \Delta_2}. \tag{7}$$

(b) For the AFM case, the energy of the diagonal intraorbital hopping excited state is

$$E^0_{\mathrm{exc}11} = 3U + 10U' - 5J_H + 2\Delta_0 + 2\Delta_1 + 4\Delta_2. \tag{8}$$

Thus, the energy gain for the AFM configuration due to the intraorbital hopping t_{11} (or t_{00}) is

$$\Delta E_{\mathrm{AFM}-11} = \frac{|\langle\psi^0_{\mathrm{exc}}|H'|\psi^0_1\rangle|^2}{E^0_1 - E^0_{\mathrm{exc}11}} = -\frac{|t_{11}|^2}{U + J_H}. \tag{9}$$

For the same AFM case, the energy of the off-diagonal hopping t_{12} excited state is

$$E^0_{\mathrm{exc}12} = 2U + 11U' - 5J_H + 2\Delta_0 + 3\Delta_1 + 3\Delta_2. \tag{10}$$

The energy gain for the AFM configuration due to the off-diagonal hopping t_{12} is

$$\Delta E_{\mathrm{AFM}-12} = \frac{|\langle\psi^0_n|H'|\psi^0_1\rangle|^2}{E^0_1 - E^0_n} = -\frac{|t_{12}|^2}{U - J_H + \Delta_1 - \Delta_2}. \tag{11}$$

The total energy gained in the AFM state from the t_{00}, t_{11}, and t_{12} terms, using the same DFT and Hund parameters as in the FM case, is

$$\Delta E_{\mathrm{AFM}} = -\frac{|t_{00}|^2}{U + J_H} - \frac{|t_{11}|^2}{U + J_H} - \frac{|t_{12}|^2}{U - J_H + \Delta_1 - \Delta_2}. \tag{12}$$

It can be shown that, for $U \gtrsim 2.17$ eV, i.e., $U/W \gtrsim 1.04$, $|\Delta E_{\mathrm{FM}}| > |\Delta E_{\mathrm{AFM}}|$. The large off-diagonal t_{12} hopping plays the key role on the dominance of ferromagnetism over antiferromagnetism. Note the important role of J_H as

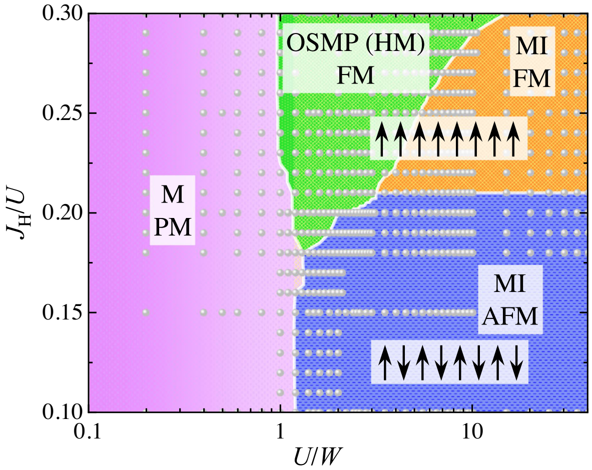

FIG. 4. DMRG phase diagram of the three-orbital Hubbard model varying U/W and J_H/U, using an $L = 16$ chain. Different phases are indicated, with the conventions metal (M), Hund metal (HM), orbital-selective Mott phase (OSMP), Mott insulator (MI), paramagnetic (PM), AFM, and FM phases. Small circles indicate specific values of data points that were investigated with DMRG. The phase boundaries should only be considered crude approximations because a mixture of competing states as well as incommensurate phases were detected near those boundaries. However, the existence of the four phases shown was clearly established, even if the boundaries are only crude estimations.

well: repeating the calculation for $J_H = 0$, the result is reversed and the AFM state wins. Varying J_H, a transition AFM-FM occurs. Specifically, for $U = 10$ eV, the critical ratio is $J_H/U \sim 0.2$ as in the density matrix renormalization group (DMRG) results next.

DMRG and phase diagram.—The magnetic phase diagram (Fig. 4) was calculated varying U/W and J_H/U using the DMRG++ code [49–53]. We found four dominant regimes in our calculations: (1) M-PM, (2) MI-AFM, (3) OSMP-FM, and (4) MI-FM. At $U/W \lesssim 1$, the system is metallic and nonmagnetic (M-PM), as expected. As U/W increases (in particular, as $U/W \gtrsim 1$), the system becomes a Mott insulator with AFM spin ordering up-down at $J_H/U \lesssim 0.21$ (MI-AFM). Increasing J_H/U, the system now enters a FM region. Interestingly, at intermediate U/W and $0.21 \lesssim J_H/U \lesssim 0.30$, due to the strong competition between J_H/U and U/W, the system is in an exotic OSMP-FM state with the selective localization of electrons on one orbital, while other orbitals remain metallic. This state was much studied recently [36,55,56] and will not be discussed here further. At both large U/W and J_H/U, the system develops a gap and becomes insulating, defining the MI-FM state of our focus. From experiments [38,39], COFS should be located at the MI-FM phase. Here, the large U renders all orbitals localized and in a high-spin state leading to the unusual FM configuration explained before via second-order perturbation theory.

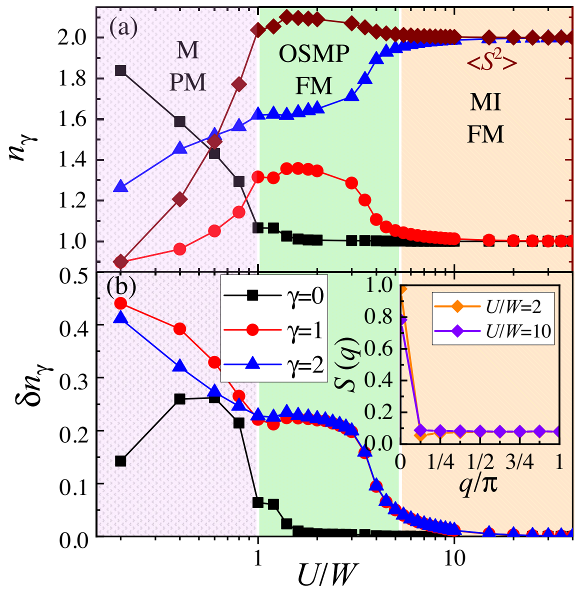

FIG. 5. (a) Orbital-resolved occupation number n_γ, mean value of the total spin squared $\langle \mathbf{S}^2 \rangle$ (in maroon color) and (b) charge fluctuations vs U/W at $J_H/U = 1/4$. Inset: spin structure factor for $U/W = 2$ and 10. Similarly, as in Fig. 4, at the boundaries phase competition renders some results slightly inaccurate. For example, the first two black points in (a) from the left in the OSMP regime are not exactly 1. Yet because their state is FM, we believe they are part of the OSMP FM rather than a new phase.

For the prototypical value $J_H/U = 1/4$, the electronic occupancy and local moment are in Fig. 5(a). In the small-U metallic PM phase, the n_γ values of all three orbitals evolve smoothly from the noninteracting limit with increasing U: the extra electron gradually transfers from sector 1 to sector 2 until a critical $U \sim W$. When $U/W \gtrsim 4$ and arriving to the MI-FM phase, the extra electron has totally transferred to γ_2, leading to $n_2 = 2$, while $n_0 = n_1 = 1$. In the MI-FM region, the fluctuations of all three orbitals are suppressed and the total spin squared, Fig. 5(a), saturates to 2, i.e., spin 1, the maximum number our study can generate (four electrons in three orbitals per site). In this sense, our results agree with powder neutron scattering that also reported a spin close to the maximum possible for Fe^{2+} [57].

The spin structure factors $S(q)$ for $U/W = 2$ and 10 are in the inset of Fig. 5(b). $S(q)$ displays a sharp peak at $q = 0$ for both $U/W = 2$ and 10, indicating FM order within the OSMP and MI regions, the latter as in experiments [38,39]. The corresponding single-particle spectra and DOS for $J_H/U = 1/4$ and $U/W = 10$ are in the Supplemental Material [48]. Orbitals γ_0 and γ_1 are half filled with a gap, while orbital γ_2 is fully filled. Then, the final gap becomes ∼2.5 eV.

Conclusions.—The iron oxychalcogenide COFS with $n = 6$ electrons per Fe was studied by DFT, by DMRG applied to a three-orbital model, and by second-order perturbation theory to gain intuitive insight. We showed that in COFS interorbital electronic hopping amplitudes can become comparable or larger than the intraorbital hoppings due to geometrical reasons, stabilizing an insulating FM state. The proposed mechanism was confirmed via DMRG. Our rich phase diagram suggests that COFS is at strong U/W, as in experiments [38,39]. The proposed mechanism requires J_H to be robust as well, as in iron superconductors. We predict that the similar chain system $\mathrm{Na_2Fe}X_2$ [58] should also exhibit FM coupling along the chain direction.

The work of L.-F. L., Y. Z., A. M., and E. D. was supported by the U.S. Department of Energy (DOE), Office of Science, Basic Energy Sciences (BES), Materials Sciences and Engineering Division. G. A. was partially supported by the Scientific Discovery through Advanced Computing (SciDAC) program funded by U.S. DOE, Office of Science, Advanced Scientific Computing Research and BES, Division of Materials Sciences and Engineering. The calculations were carried out at the University of Tennessee Advanced Computational Facility (ACF).

[1] P. W. Anderson, Phys. Rev. **115**, 2 (1959).
[2] J. B. Goodenough, *Magnetism and the Chemical Bond* (Wiley Interscience, New York, 1963), Vol. 1.
[3] P. W. Anderson, in *Solid State Physics* (Elsevier, New York, 1963), Vol. 14, pp. 99–214, https://doi.org/10.1016/S0081-1947(08)60260-X.
[4] L.-F. Lin, N. Kaushal, C. Sen, A. D. Christianson, A. Moreo, and E. Dagotto, Phys. Rev. B **103**, 184414 (2021).
[5] H. Weihe and H. U. Güdel, Inorg. Chem. **36**, 3632 (1997).
[6] The present study suggests that COFS host the competition between the mechanism [Figs. 1(a) and 1(c)]. Interestingly, the abnormally large interorbital hopping amplitude together with large J_H allows the FM kinetic mechanism [Fig. 1(c)] to dominate over Fig. 1(a).
[7] E. Dagotto, T. Hotta, and A. Moreo, Phys. Rep. **344**, 1 (2001).
[8] M. Mayr, A. Moreo, J. A. Vergés, J. Arispe, A. Feiguin, and E. Dagotto, Phys. Rev. Lett. **86**, 135 (2001).
[9] A. Moreira dos Santos, A. K. Cheetham, T. Atou, Y. Syono, Y. Yamaguchi, K. Ohoyama, H. Chiba, and C. N. R. Rao, Phys. Rev. B **66**, 064425 (2002).
[10] Y. K. Wakabayashi, Y. Krockenberger, N. Tsujimoto, T. Boykin, S. Tsuneyuki, Y. Taniyasu, and H. Yamamoto, Nat. Commun. **10**, 535 (2019).
[11] J. Zhang, X. Cai, W. Xia, A. Liang, J. Huang, C. Wang, L. Yang, H. Yuan, Y. Chen, S. Zhang *et al.*, Phys. Rev. Lett. **123**, 047203 (2019).
[12] J. Q. Yan, J. S. Zhou, and J. B. Goodenough, Phys. Rev. B **70**, 014402 (2004).
[13] V. V. Mehta, N. Biskup, C. Jenkins, E. Arenholz, M. Varela, and Y. Suzuki, Phys. Rev. B **91**, 144418 (2015).
[14] Q. Zhang, A. Gao, F. Meng, Q. Jin, S. Lin, X. Wang, D. Xiao, C. Wang, K.-j. Jin, D. Su *et al.*, Nat. Commun. **12**, 1853 (2021).
[15] A. A. Taskin, A. N. Lavrov, and Y. Ando, Phys. Rev. Lett. **90**, 227201 (2003).
[16] H. Das, U. V. Waghmare, T. Saha-Dasgupta, and D. D. Sarma, Phys. Rev. Lett. **100**, 186402 (2008).
[17] H. L. Feng, Z. Deng, C. U. Segre, M. Croft, S. H. Lapidus, C. E. Frank, Y. Shi, C. Jin, D. Walker, and M. Greenblatt, Inorg. Chem. **60**, 1241 (2020).
[18] M. A. McGuire, H. Dixit, V. R. Cooper, and B. C. Sales, Chem. Mater. **27**, 612 (2015).
[19] C. Gong, L. Li, Z. Li, H. Ji, A. Stern, Y. Xia, T. Cao, W. Bao, C. Wang, Y. Wang *et al.*, Nature (London) **546**, 265 (2017).
[20] Z. Huang, D. Liu, A. Mansikkamäki, V. Vieru, N. Iwahara, and L. F. Chibotaru, Phys. Rev. Research **2**, 033430 (2020).
[21] M. Steiner, J. Villain, and C. Windsor, Adv. Phys. **25**, 87 (1976).
[22] P. W. Anderson, Phys. Rev. **79**, 350 (1950).
[23] J. B. Goodenough, Phys. Rev. **100**, 564 (1955).
[24] J. B. Goodenough, J. Phys. Chem. Solids **6**, 287 (1958).
[25] J. Kanamori, J. Phys. Chem. Solids **10**, 87 (1959).
[26] K. Kuroki, S. Onari, R. Arita, H. Usui, Y. Tanaka, H. Kontani, and H. Aoki, Phys. Rev. Lett. **101**, 087004 (2008).
[27] B. Pandey, Y. Zhang, N. Kaushal, R. Soni, L.-F. Lin, W.-J. Hu, G. Alvarez, and E. Dagotto, Phys. Rev. B **103**, 045115 (2021).
[28] L.-F. Lin, N. Kaushal, Y. Zhang, A. Moreo, and E. Dagotto, Phys. Rev. Mater. **5**, 025001 (2021).
[29] L.-F. Lin, Y. Zhang, A. Moreo, E. Dagotto, and S. Dong, Phys. Rev. Lett. **123**, 067601 (2019).
[30] Y. Zhang, L.-F. Lin, A. Moreo, G. Alvarez, and E. Dagotto, Phys. Rev. B **103**, L121114 (2021).
[31] Y. Zhang, L.-F. Lin, A. Moreo, S. Dong, and E. Dagotto, Phys. Rev. B **100**, 184419 (2019).
[32] Y. Zhang, L.-F. Lin, A. Moreo, S. Dong, and E. Dagotto, Phys. Rev. B **101**, 144417 (2020).
[33] Y. Zhang, L.-F. Lin, A. Moreo, S. Dong, and E. Dagotto, Phys. Rev. B **101**, 174106 (2020).
[34] J. Herbrych, J. Heverhagen, G. Alvarez, M. Daghofer, A. Moreo, and E. Dagotto, Proc. Natl. Acad. Sci. U.S.A. **117**, 16226 (2020).
[35] B. Pandey, L.-F. Lin, R. Soni, N. Kaushal, J. Herbrych, G. Alvarez, and E. Dagotto, Phys. Rev. B **102**, 035149 (2020).
[36] N. Patel, A. Nocera, G. Alvarez, A. Moreo, S. Johnston, and E. Dagotto, Commun. Phys. **2**, 64 (2019).
[37] J. Herbrych, J. Heverhagen, N. D. Patel, G. Alvarez, M. Daghofer, A. Moreo, and E. Dagotto, Phys. Rev. Lett. **123**, 027203 (2019).
[38] E. E. McCabe, D. G. Free, and J. S. Evans, Chem. Commun. **47**, 1261 (2011).
[39] E. E. McCabe, C. Stock, J. L. Bettis, M. H. Whangbo, and J. S. O. Evans, Phys. Rev. B **90**, 235115 (2014).
[40] G. Kresse and D. Joubert, Phys. Rev. B **59**, 1758 (1999).
[41] P. E. Blöchl, Phys. Rev. B **50**, 17953 (1994).
[42] J. P. Perdew, A. Ruzsinszky, G. I. Csonka, O. A. Vydrov, G. E. Scuseria, L. A. Constantin, X. Zhou, and K. Burke, Phys. Rev. Lett. **100**, 136406 (2008).

[43] N. Marzari and D. Vanderbilt, Phys. Rev. B **56**, 12847 (1997).

[44] A. A. Mostofi, J. R. Yates, Y.-S. Lee, I. Souza, D. Vanderbilt, and N. Marzari, Comput. Phys. Commun. **178**, 685 (2008).

[45] Note that we calculate hoppings and crystal fields based on DFT without including interaction effects, as most commonly done in the literature. Alternatively, we could have calculated these parameters using DFT in the FM spin background relevant for COFS. But this procedure would have not allowed us to provide the entire phase diagram, including non-FM phases, as shown in the DMRG section. Another interesting observation is that in Fig. 2 in the Supplemental Material, we noticed that even at very large Hubbard coupling the bandwidth of, e.g., the lower and upper Hubbard bands remain similar in value to the original noninteracting bandwidth. Thus, contrary to naive expectation, the bands do not flatten at large U, although they seem flat when compared to the large gaps generated by U.

[46] The Hubbard-like model commonly discards the FM direct exchange as mentioned by Ku *et al.* [47], but direct exchange could be legitimately omitted in our case since the kinetic exchange dominates over the direct exchange.

[47] W. Ku, H. Rosner, W. E. Pickett, and R. T. Scalettar, Phys. Rev. Lett. **89**, 167204 (2002).

[48] See Supplemental Material at http://link.aps.org/supplemental/10.1103/PhysRevLett.127.077204 for more details of the method, hopping matrix, and spectrum and DOS plot, which includes Refs. [38–44,49–54].

[49] S. R. White, Phys. Rev. Lett. **69**, 2863 (1992).

[50] S. R. White, Phys. Rev. B **48**, 10345 (1993).

[51] U. Schollwöck, Rev. Mod. Phys. **77**, 259 (2005).

[52] K. A. Hallberg, Adv. Phys. **55**, 477 (2006).

[53] G. Alvarez, Comput. Phys. Commun. **180**, 1572 (2009).

[54] K. Momma and F. Izumi, J. Appl. Crystallogr. **44**, 1272 (2011).

[55] R. Yu, H. Hu, E. M. Nica, J.-X. Zhu, and Q. Si, Front. Phys. **9**, 578347 (2021).

[56] J. Rincón, A. Moreo, G. Alvarez, and E. Dagotto, Phys. Rev. Lett. **112**, 106405 (2014).

[57] The total spin square equals 2, which means $\mathbf{S} = 1$ and spin moment is 2 μ_B for three orbitals, in agreement with the high-spin state observed by experiment. If we consider the five orbitals, then the final spin magnetic moment can be roughly estimated as 4 μ_B, which is slightly larger but close to the experimental observed value $\sim$3.14–3.33 μ_B [38,39].

[58] P. Stüble, S. Peschke, D. Johrendt, and C. Röhr, J. Solid State Chem. **258**, 416 (2018).